

Time-Dependent Photoionization in a Dusty Medium. III: The effect of dust on the photoionization of metals

Davide Lazzati¹ & Rosalba Perna^{2,3}

¹ *Institute of Astronomy, University of Cambridge, Madingley Road, Cambridge CB3 0HA, England*

² *Harvard Society of Fellows, 78 Mt. Auburn Street, Cambridge, MA 02138*

³ *Harvard-Smithsonian Center for Astrophysics, 60 Garden Street, Cambridge, MA 02138*

e-mail: lazzati@ast.cam.ac.uk; rperna@cfa.harvard.edu

29 October 2018

ABSTRACT

We use the time-dependent photoionization and dust destruction code developed by Perna & Lazzati (2002) to study the time evolution of the medium in a dusty gaseous cloud illuminated by a bright central source that sets on at time zero. We study the case of a bright source, which lasts for a time scale much smaller than the recombination and dust creation time scales. For this reason an equilibrium is never reached. We show that the presence of dust and its properties, such as its composition, can have a big effect on the time scale for the evaporation of the soft X-ray absorption, in particular for ionizing sources with hard spectra. We discuss the profile of evaporation of the soft X-ray absorbing column, as well as how the apparent ionization state of the cloud evolves in time. We finally consider the apparent metallicity of the cloud that is left behind as a function of the cloud and ionizing source properties.

1 INTRODUCTION

The measurement of the amount of absorption in the soft X-ray band is highly informative about the amount and physical state (e.g. temperature, ionization parameter) of the material that lies along the line of sight between a source and an observer. Observed spectra are usually analyzed under the assumption that the absorber is in equilibrium, either a thermal or photoionization equilibrium (Morrison & McCammon 1983; Done et al. 1992; Zdziarski et al. 1995). This assumption is justified if the source that is studied is constant or if its variability time scale is much longer than the electron recombination time scale of the absorbing material. There are however many variable sources in the universe that do not fulfill this condition. Among them it is worth mentioning X-ray transients (see e.g. Schwarz 1973), variable AGNs (see, e.g. Risaliti, Elvis & Nicastro 2002) and especially gamma-ray bursts (Perna & Loeb 1998; Lazzati & Perna 2002, hereafter LP02). In all these cases, out to a certain distance, photoionization acts as a destructive mechanism: each time a photon is absorbed an electron is stripped, and therefore the state of the absorber and its absorption properties are modified.

LP02 (see also Schwarz 1973) analyzed by means of numerical simulations the absorption properties of a gaseous medium suddenly illuminated by a strong photon source with a power-law spectrum. They followed the ionization state of the 12 astrophysically relevant elements and hydrogen producing time resolved transmittance spectra to be compared with the data. In many cases, however, assuming that all the interstellar medium (ISM) is in a gaseous phase is not accurate. There can be molecules (that do not

have sizable affect on the X-ray opacity of the medium, see Perna, Lazzati & Fiore 2002, hereafter Paper II) and, most importantly, there can be dust grains. These in particular are relevant to X-ray absorption since a large fraction of heavy metals can be condensed in silicate dust grains (Savage & Mathis 1979; Laor & Draine 1993). The presence of dust grains in the ISM modifies the X-ray absorption properties in two main ways. First, the presence of dust increases the opacity for UV photons, that cannot therefore contribute to the ionization of metals by stripping their external electrons. Most importantly, the metals contained into a dust grain are shielded to photoionization, so that they can survive in an almost neutral state for a much longer time than the same atom in gaseous phase.

We (Perna & Lazzati 2002, hereafter Paper I) have developed a code that computes the time-dependent absorption properties of a dusty ISM (possibly enriched with H_2 molecules) as a function of time under the illumination of a power-law ionizing continuum that evaporates dust grains, dissociates molecules and ionizes atoms. The code and the physical processes considered are fully described in Paper I. The properties of absorption in the optical range are analyzed in a second paper (Paper II). Here, we focus on the properties of the absorber in the X-ray range, and on how the presence of dust influences the evolution of the opacity under different conditions.

In § 2, we briefly introduce the code and describe the outputs that will be used here, in § 3 we discuss the main effects of the presence of dust while in § 4 we study how these effects depend on the spectrum of the central ionizing source. In § 5 we study how the residual column density can be quantified with a single parameter and in § 6 we consider the

arXiv:astro-ph/0212105v2 5 Dec 2002

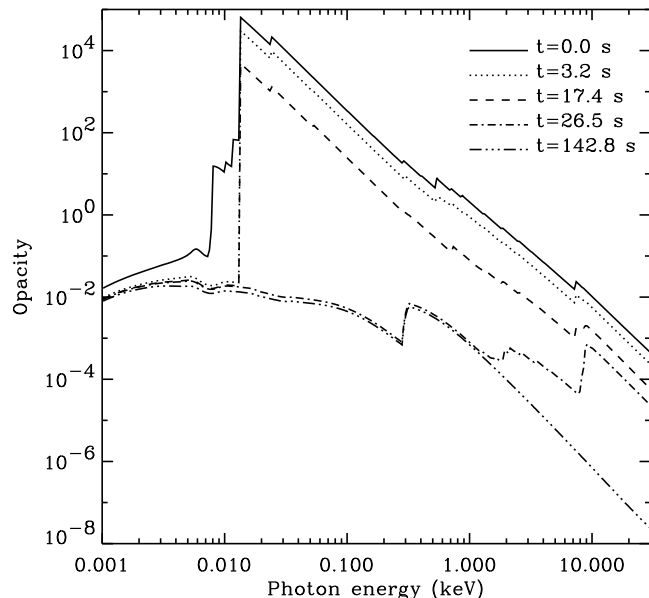


Figure 1. The opacity as a function of frequency from optical to X-rays in several time shots after the ionizing continuum onset. The absorbing medium is a spherical cloud with radius $R = 10^{18}$ cm and uniform density $n = 10^4$ cm $^{-3}$ ($N_H = 10^{22}$ cm $^{-2}$) with the source at its centre. Abundances are set to the solar value and the dust-to-gas mass fraction is 0.01 (the average Galactic value).

shape of the transmitted spectrum and in particular whether a high ionization parameter can be detected at intermediate stages. In § 7, we consider the different ionization time scales of the various elements and the possible effects that this can have on the estimate of metallicity derived from the fit of the relative opacities. Finally, in § 8, we summarize and discuss our results.

2 CODE OUTPUTS

The code we used for this analysis is fully described in Paper I, where the physics of dust evaporation is discussed in detail. We consider two species of grains: graphite, purely composed of carbon atoms, and silicates, made of MgFeSiO $_4$ molecules¹. The effects of dust opacity and destruction were implemented into a widely used photoionization code (Raymond 1979; Perna, Raymond & Loeb 2000).

Among the various outputs of the code described in Paper I, we will mainly use in this paper the radially integrated opacity as a function of frequency, which we will call “spectral opacity distribution” (SOD). An example output of the code is shown in Figs. 1 and 2, where the opacity is plotted versus frequency for a uniform cloud² with radius $R = 10^{18}$ cm, density $n = 10^4$ cm $^{-3}$, solar metallicity and

¹ As discussed in Paper I, the silicate grain should be rather thought as a lattice with average elemental abundances described by this formula.

² Note that in all the code runs presented here the term cloud refers to the uniform cloud of gas that surrounds the source (which is at its centre) and not to a cloudlet at a certain distance from the source.

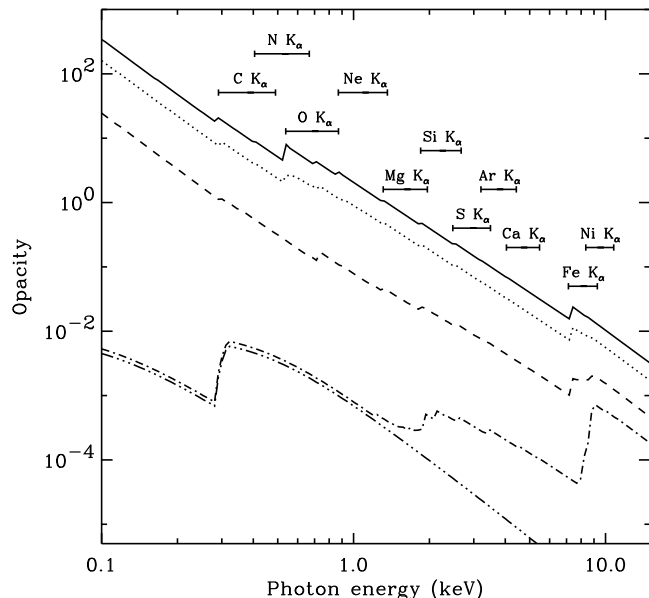


Figure 2. Zoom of Fig 1 in the X-ray ([0.1–15] keV) range. Horizontal bars show the range of K_α photoionization edge frequencies for the considered elements (besides H and He) from neutral to H-like.

dust-to-gas ratio $d_k = 1$, where d_k is the ratio between the mass of dust and the mass of gas, normalized to the local galactic value $d_{k, \text{local}} = 0.01$. A cloud with solar dust-to-gas ratio will therefore have $d_k = 1$. The central source sets on at observed time $t = 0$ with a constant [1 eV–100 keV] luminosity of $L = 10^{50}$ erg s $^{-1}$ and a power-law spectrum $L(\nu) \propto \nu^0$, which correspond to a photon luminosity of $Q_H \approx 7.2 \times 10^{57}$ s $^{-1}$. This choice of luminosity and spectrum is appropriate if the central source is a Gamma-Ray Burst. This code can be applied in principle to different objects, such as AGNs, especially to describe the effect of periods of enhanced activity on the surrounding environment. A rather smaller luminosity $L \sim 10^{40-45}$ erg s $^{-1}$ should be adopted in this case, and we will discuss below (see § 3.1) in which cases the results presented here can be simply rescaled to the case of AGNs (see also Paper II).

In Fig. 3 we show a comparison between the SOD of a cold gaseous cloud as implemented in our code (based on Reilman & Manson 1979) and two more recent atomic datasets (Morrison & McCammon 1983 and Verner & Yakovlev 1995). Here and in the following we will use indifferently the term *cold* or *neutral* that will have the same meaning of non ionized. The agreement is reasonable, even though some discrepancy in the very soft X-ray range can be seen. This is mainly due to a different shape for the H and He photoionization cross-sections at frequencies much larger than the threshold.

3 THE EFFECT OF DUST ON THE PHOTOIONIZATION OF METALS

As mentioned in the introduction, the presence of dust has mainly two effects on the photoionization rate of the ISM. The first effect is that of reducing the transmitted UV flux. This causes a delay in the photo-ejection of higher orbital

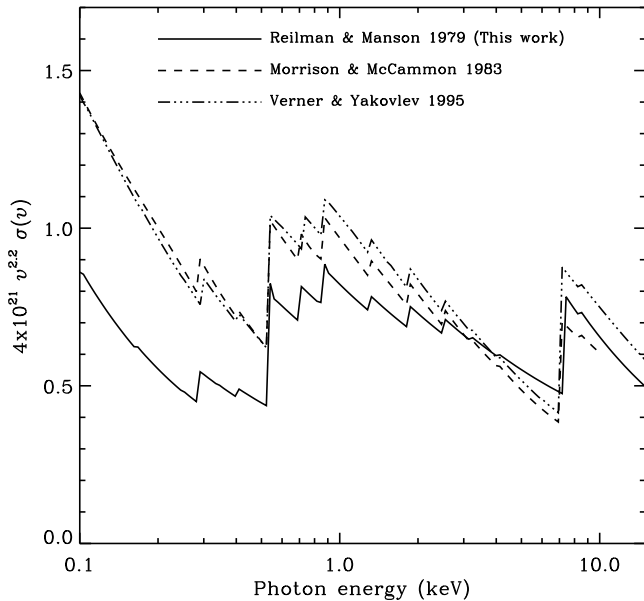


Figure 3. Comparison of the cross sections used in the code (Reilman & Manson 1979) with two other widely used atomic datasets (Morrison & McCammon 1983 and Verner & Yakovlev 1995). Differences, up to a factor 1.5, are present especially in the range where the absorption is dominated by Helium. Much better agreement is obtained at larger frequencies.

electrons which is of relatively small importance. In fact, in the X-ray regime, the opacity is mainly due to K -shell electrons that are not sensitive to UV radiation.

A much more important effect is that of shielding that the grain has on the metals contained inside the grain itself. This is not due to the fact that the grain is opaque to X-ray radiation (a condition that is satisfied only in the very large grains that do not have a sizable contribution on the absorption) but to the capacity of the grain itself to sustain an electric potential large enough to avoid the ejection from the grain of photoelectrons that are therefore re-captured by the atom that was stripped. In order to understand when and why this happens it's worth reviewing the grain destruction mechanisms described in Paper I, to which we remind the reader for a more thorough analysis.

We consider dust destruction due to two mechanisms: thermal sublimation and ion field emission (IFE). The first mechanism is active when the flux of UV and soft X-ray photons is large enough to heat the grain above a critical temperature of the order of several thousand Kelvin. The condition is realized if either the grain is close to the photon source or the spectrum is soft (see § 4). In these conditions the grain evaporates by ejecting neutral or singly ionized atoms in a time scale that is much smaller than the ionization time scale for the inner electrons. For this reason the X-ray opacity depends only weakly on whether the atom was initially bound to a grain or in gaseous phase.

If the grain temperature is not kept large enough, the thermal sublimation time scale increases exponentially and a different mechanism (IFE) can set in. In particular, if the ionizing continuum has a hard spectrum, intermediate-hard X-ray photons can ionize the grain without sizably heating it. Due to the strength of the molecular bonds, the charged

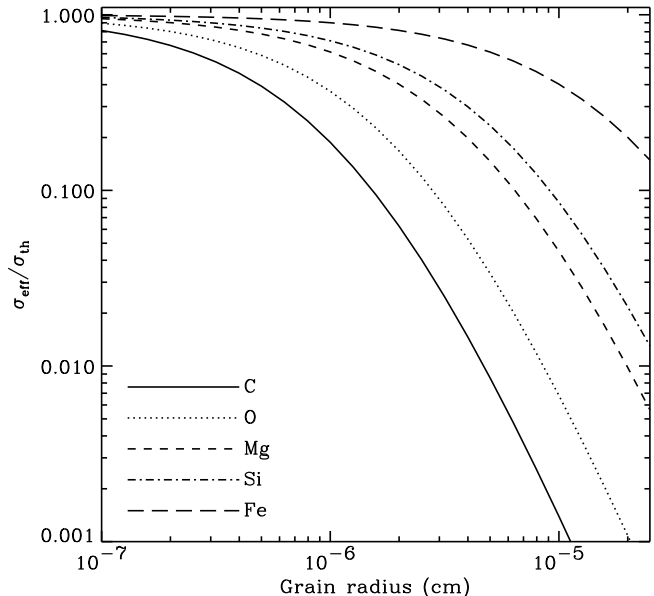


Figure 4. Effective cross section for K_α photoionization of elements in maximally charged grains vs. the grain radius. The effective cross section is shown divided by the cross section of the same atom in gaseous phase, in order to emphasize the effect of metals contained in grains versus those in gaseous phase.

grain can resist up to a threshold potential of $3a_{-5}$ kV (Waxman & Draine 2000) where a_{-5} is the grain radius in units of 10^{-5} cm. After this threshold is overcome, the grain reacts to any further ionization by ejecting an ion. Consider, however, a photon with $h\nu = 0.3$ keV and a graphite grain. The photon has energy large enough to photoionize an isolated carbon atom by stripping a K electron that has an ionization energy of 0.291 keV. If however the carbon atom is bound in a charged graphite grain, the photoelectron will be unable to escape from the grain due to the large potential barrier and will consequently recombine in a very short time with a carbon ion. A carbon atom bound to a maximally charged graphite grain of radius a has therefore an effective ionization energy:

$$h\nu_{\text{eff}} = h\nu_{\text{th}} + 3a_{-5} \text{ keV} \quad (1)$$

where $h\nu_{\text{th}}$ is the ionization potential of the isolated atom. This will correspond also to a decrease in cross section:

$$\frac{\sigma_{\text{eff}}}{\sigma_{\text{th}}} \sim \left(1 + \frac{3a_{-5} \text{ keV}}{h\nu_{\text{th}}}\right)^{-3} \quad (2)$$

where σ_{th} is the threshold cross section for photoionization of an isolated atom. The decrease in the cross section, which is proportional to the increase in photoionization time scale (Lazzati, Perna & Ghisellini 2001), is shown in Fig. 4 for C, O, Mg, Si and Fe, the atoms that we consider as components of graphite and silicates. In the figure, the proper shape of the cross section function is taken into account, rather than the simplified power-law behavior of Eq. 2. It is clear that, the lower the photoionization potential, the larger is the decrease of the effective cross section, and therefore graphite grains will be more effective in shielding the photoionization with respect to silicates, in which iron is almost unaffected.

Another effect in competition with IFE grain destruction is the recombination of free electrons onto the charged

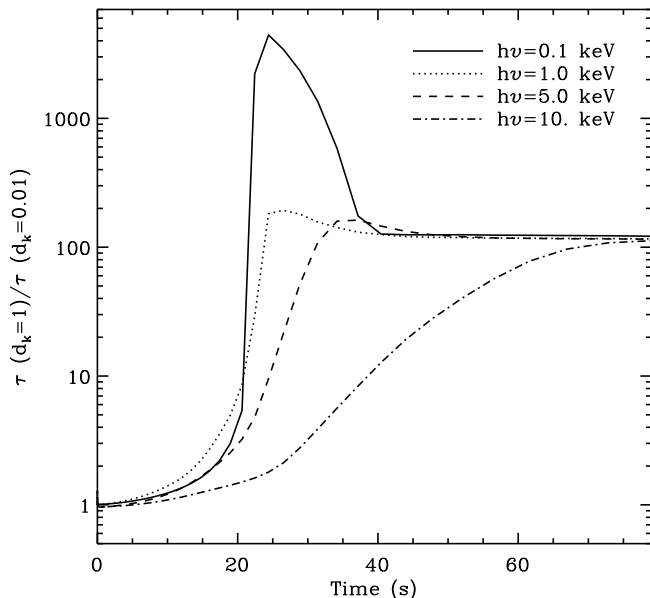


Figure 5. The effect of dust in the evolution of the X-ray opacities. The figure shows a comparison between the opacity at various frequencies for a simulation with standard dust-to-gas ratio and a simulation with a hundred times less dust. In both the simulations the absorbing medium is a spherical cloud with radius $R = 10^{18}$ cm and uniform density $n = 10^4$ cm $^{-3}$ ($N_H = 10^{22}$ cm $^{-2}$). Abundances are set to the solar value.

grain, when its charge is below the threshold for the IFE effect (Fruchter et al. 2001; Paper I). Even if the importance of recombination with respect to ionization depends on the type of grain considered and on the spectrum of the ionizing source, one can roughly write the ratio of the time scales as:

$$\frac{dN_{\text{ion}}/dt}{dN_{\text{rec}}/dt} \sim 10^{-8} \xi T_5^{1/2} \quad (3)$$

where $\xi \equiv L/(nR^2)$ is the ionization parameter (see also § 6) and T_5 is the electron temperature in units of 10^5 K. The effect of recombination can be therefore neglected in our computations (it is marginally important for the largest and densest cloud, see § 6), but should be taken into account when considering less luminous ionizing sources and/or absorbers at larger distances.

The effect of dust in changing the ionization time scales is shown in Fig. 5, where the opacities at selected frequencies versus time are compared for two sets of simulations: one with solar dust-to-gas ratio ($d_k = 1$) and the other with a dust depletion of a factor 100 ($d_k = 0.01$). The opacity in the latter, “no-dust” simulation decreases on a smaller time scale, and in fact after ~ 20 seconds, the opacity in the dusty case can be more than on thousand times larger than in the no-dust case (see the 0.1 keV line in Fig. 5). At very late times, the SOD in both simulations is dominated by opacity due to unevaporated graphite grains, and therefore in the no-dust simulation is 100 times smaller than in the dusty one (see however §4 for how the effect is reduced with a softer spectrum). The effect can also be seen in Figs. 1 and 2: the lower line, which shows the opacity at the largest time, is completely dominated by the opacity due to the large graphite grains, which survived destruction at large radii by the shielding mechanism. Should such an extreme condition

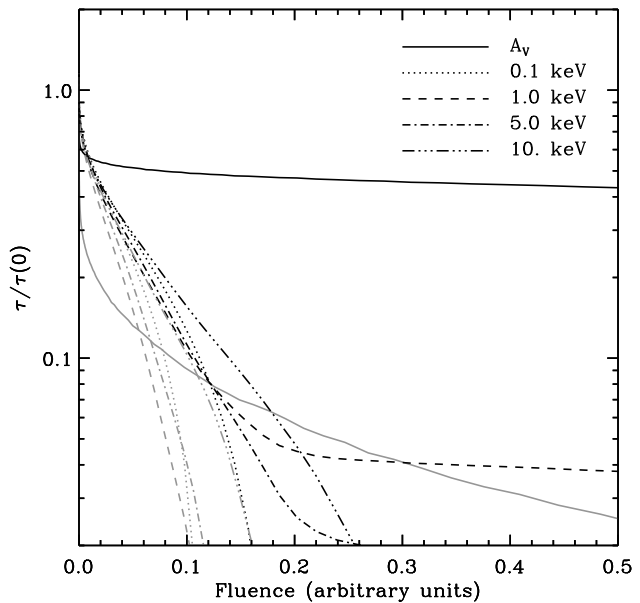


Figure 6. Opacity as a function of fluence for a cloud surrounding a uniform source of ionizing photons (dark lines) and a source with 10 times larger peak luminosity but which is on only for 10% of the time, so that the two sources have the same average fluence $\mathcal{F}(t)$. See §3.1 for more details.

be realized in a real source, it may be recognizable, being characterized by a typical N_H/A_V ratio (see also Paper I and II)

$$\left(\frac{N_H}{A_V}\right)_{\text{graphite}} \sim 10^{20} \text{ cm}^{-2} \quad (4)$$

which is roughly ten times smaller than for a cold gas with solar metallicity and dust content. Moreover, it should be characterized by a prominent³ absorption edge at the threshold of neutral carbon: $h\nu = 0.291$ keV.

Such a phase of the ISM, in which dust grains coexist with a fully ionized gas, may not be an equilibrium condition. In fact, the electron temperature of the free electrons will be around $T \sim 10^5$ K (Perna et al. 2000), a temperature large enough to sublimate the grains. The energy input rate of the grains due to the electron bombardment is $\dot{E} = \pi a^2 n_e v_e \epsilon_e$ where v_e is the electron mean velocity and ϵ_e their mean energy. This heating term is always much smaller than the black-body cooling term $\dot{E} = 4\pi a^2 \sigma T^4$. The grain is therefore stable in the hot electron bath, at least for the time scale of interest in this paper.

3.1 Breaking the time, size and luminosity degeneracy and the effect of a variable source

When a purely gaseous cloud is considered, it can be shown that the ionization state of the cloud depends on the local fluence rather than on the flux and time elapsed since the source onset independently (LP02). This is an important conclusion, which holds in both the optically thin and thick cases, since it allows to apply the results of a simulation

³ The edge may become less and less important for very big grains of radius larger than $\sim 1\mu\text{m}$.

Symbol	Explanation
N_X	Total column of the element X , irrespective of its ionization state, even if completely stripped off all the electrons.
$N_{X>}$	Total photo-absorbing column of the element X , i.e. with at least one associated electron.
$N_{[X]}$	Column density as measured from soft X-ray absorption, under the assumption of a cold intervening medium.
R	Radius of the surrounding cloud
n	Density of the absorbing medium
L	Luminosity of the power-law ionizing continuum in the [1 eV–100 keV] range
α	Spectral index of the power law continuum ($L(\nu) \propto \nu^{-\alpha}$)
a	Radius of dust particles
ξ	Ionization parameter of the gas
d_k	Dust content parameter: ratio of dust-to-gas mass densities relative to the solar value

Table 1. Explanation of symbols used throughout the text.

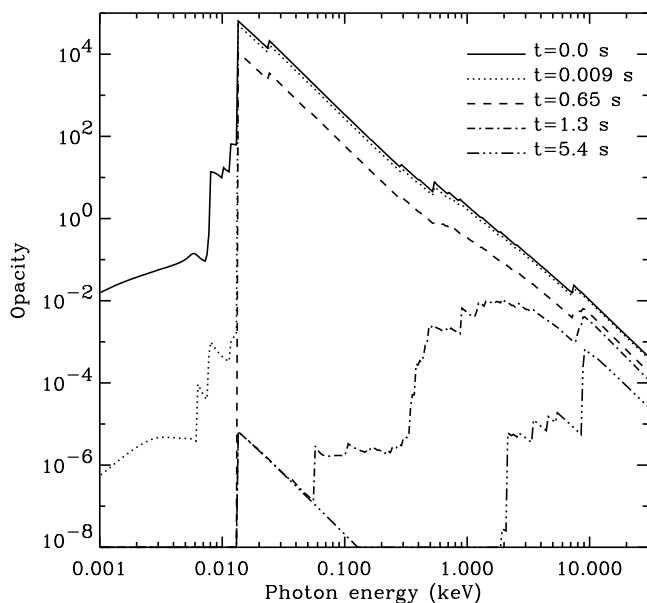


Figure 7. Same as Fig 1 but for $\alpha = 0.5$.

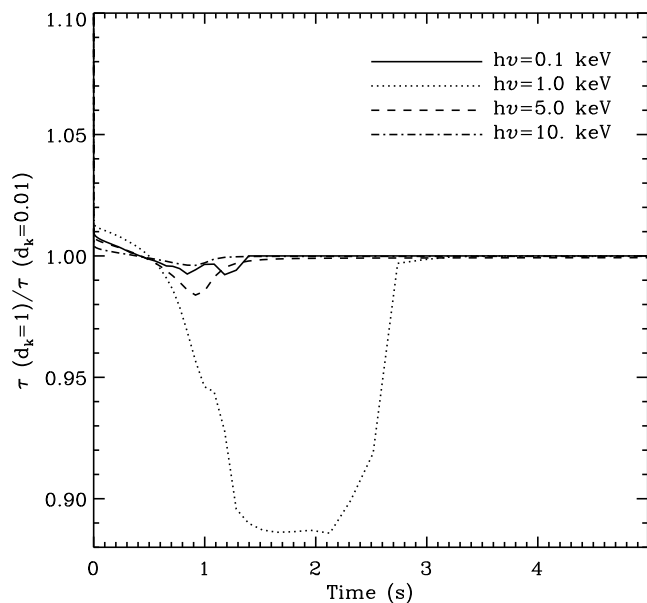


Figure 8. Same as Fig 5 but for $\alpha = 0.5$.

with a given parameter set to a different cloud geometry and input luminosity (see Eq. 1 in LP02). This relation also implies that a simulation with constant flux can be adapted for a variable source when the time is properly defined (see discussion in LP02). Moreover, a simulation with a given luminosity can be adapted to any other luminosity by simply rescaling the time, provided that it does not become longer than the recombination time scale.

When dust grains are introduced as a component of the absorbing medium, the degeneracy is broken and these scaling laws are no more valid. This is due to the fact that the degree of destruction of a dust particle does not depend uniquely on the number of photons that it absorbed, but also on the rate with which the photons have been absorbed. This is due to the fact that dust particles can radiatively cool and have a well defined temperature, the mean value of which is set by a balancing of the heating and cooling rates. For this reason, a highly variable source will be much more effective in destroying dust than a uniform one with the same total energy and overall duration.

The bottom line of this is that two luminosity and geometrical setup are now equivalent if i) the column density is the same and ii) the local flux is the same, i.e. $L_1/R_1^2 = L_2/R_2^2$, where L_1 and L_2 are the luminosity of the

central sources and R_1 and R_2 the cloud radii in the first and second simulation, respectively. In other words, the results shown in Fig. 1 can be applied to an AGN with the same spectrum but luminosity $L = 10^{44}$ erg s $^{-1}$ surrounded by a cloud of radius $R = 10^{15}$ cm and density $n = 10^7$ cm $^{-3}$.

This holds for a uniform luminosity, while additional complications are required in the case of a variable source. In Fig. 6 we show the effect of variability in the ionizing luminosity for our standard cloud with radius $R = 10^{18}$ cm, density $n = 10^4$ cm $^{-3}$ and standard dust-to-gas ratio $d_k = 1$. The central source has, in both cases, a power-law spectrum $L(\nu) \propto \nu^0$. With black lines we show the opacity as a function of fluence, for selected frequencies, for a source that turns on at $t = 0$ and then radiates uniformly in time with a luminosity $L = 10^{50}$ erg s $^{-1}$. With gray lines, we show the opacity as a function of fluence for a source that has a peak luminosity ten times larger, but is intermittent after the onset, being active only for 10% of the time. The two sources have, on average, the same fluence at time t , so that the x-axis of the figure is proportional to the elapsed time for both sources. For this reason, the black and gray lines would overlap for a purely gaseous cloud. In the variable source case, however, dust grains are held at a much larger temperature, so that they can evaporate much faster. This is clearly

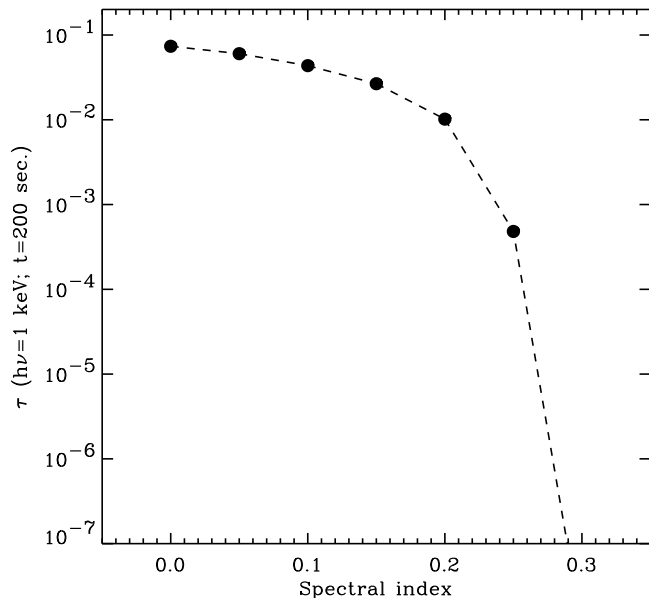


Figure 9. Late time opacity at 1 keV for a set of simulations with different spectral slopes of the ionizing continuum. The absorbing cloud is always characterized by $R = 10^{18}$ cm, $n = 10^4$ cm $^{-3}$ and $d_k = 1$. The opacity at 1 keV at $t = 200$ seconds is dominated by residual graphite grains in all simulations with $\alpha \lesssim 0.25$, while vanishes for softer spectra. See text for more details.

visible by comparing the solid lines in Fig. 6, which show the absorption in the optical V band, largely dominated by dust: it is asymptotically more than ten times smaller for the variable source than for the steady one.

4 DEPENDENCE ON SPECTRAL INDEX

The ionization state of the absorbing medium and the effectiveness of an ionizing flux in destroying dust grains depend strongly on the spectral energy distribution (SED) of the ionizing continuum. A softer spectrum will be more effective in destroying dust through thermal sublimation, while a hard spectrum will photoionize metals with good efficiency, but will leave most of the dust grains unaffected. In both cases, the SOD will be at the end very different from the initial one.

A very soft spectrum will leave behind a dust clean environment, with opacity largely suppressed at all frequencies but for the keV band, in which residual absorption from iron may still be present. On the other hand, a very hard spectrum will initially suppress the high frequency opacity until only dust grains are left which resist to further destruction thanks to the potential barrier discussed above. The different behaviors can be seen by comparing the figures obtained with different spectra. We have produced figures for power-law incident spectra $L(\nu) \propto \nu^{-\alpha}$, with luminosity $L = 10^{50}$ erg s $^{-1}$ in the [1 eV–100 keV] band. The spectral index was either $\alpha = 0$, which should reproduce the low frequency SED of a typical GRB or $\alpha = 0.5$, which should be more suited for a GRB with an optical flash⁴ (see also

Draine & Hao 2002). Fig. 1, 2 and 5 have been produced with the harder spectrum, while Fig. 7 and 8 are relative to the softer one.

Of particular interest is the comparison of Fig 1 with Fig 7. Both figures show the SOD of the same cloud in several time shots, but the former is ionized by a hard spectrum, while the latter is ionized by a softer one. Note that the times at which the SOD are shown are different, since the soft spectrum has a larger number of photons and is therefore a more efficient source of ionization. The dotted line, in both figures, shows the evolution of the SOD at early times, when the absorption properties of the cloud start to be modified. Comparing the dotted lines in Figs. 1 and 7 above and below the Lyman limit, it is easy to note how the soft spectrum is effective in evaporating dust particles. In comparison, a harder spectrum is much less effective, so that at late times the opacity is dominated by dust grains (dash-dotted lines in Fig. 1) while in Fig. 7 only a residual iron opacity is left at late times.

The hardness of the spectrum is also an extremely important parameter in evaluating to which extent the presence of dust influences the evolution of the X-ray opacity (comparison of Figs. 5 and 8). In fact, a soft spectrum efficiently destroys dust grains before the ionization state of the atoms in the gaseous phase is modified and therefore the ionization of elements takes place in a gas free environment even if it started with a sizable amount of dust. On the other hand, if the spectrum is not soft enough to destroy dust grains, the presence of dust (which is initially virtually undetectable from an X-ray spectrum) has a tremendous importance in determining the evolution of the X-ray SOD (see Fig. 5). The key parameter is therefore the ratio of the photoionization time scale to the grain destruction time scale which is a function of the spectral index of the spectrum and of the distance from the source (or the source luminosity).

It is also important to note that the amount of dust that is leftover for a cloud with a given geometry and density and for a certain ionizing luminosity is a threshold effect. Either the ionizing flux is capable of destroying all the dust grains or most of them are left behind, the intermediate situation being possible only in a very limited range of spectral shapes. In Fig 9 we show the opacity at 1 keV at the largest simulated time ($t = 200$ s) as a function of the spectral index α in a set of simulations for which only α is varied. The geometry of the absorbing cloud is given by $R = 10^{18}$ cm, $n = 10^4$ cm $^{-3}$ and $d_k = 1$ while the central source has a luminosity $L = 10^{50}$ erg s $^{-1}$. The choice of plotting the opacity at this frequency is due to the fact that at late times (in this case 200 seconds) the opacity at 1 keV (if any) is dominated by absorption by dust particles (mostly big graphite grains, see Fig. 1). For spectra softer than $\alpha = 0.25$, all the grains are destroyed and there is no residual opacity, while for harder spectra a considerable fraction of grains is left behind.

5 THE MEASURE OF THE RESIDUAL COLUMN DENSITY

As discussed in LP02, it is important to convert the result of the simulations, which contain very detailed informations

⁴ In this case the photon luminosity would be $Q_H \approx 2 \times 10^{59}$ s $^{-1}$.

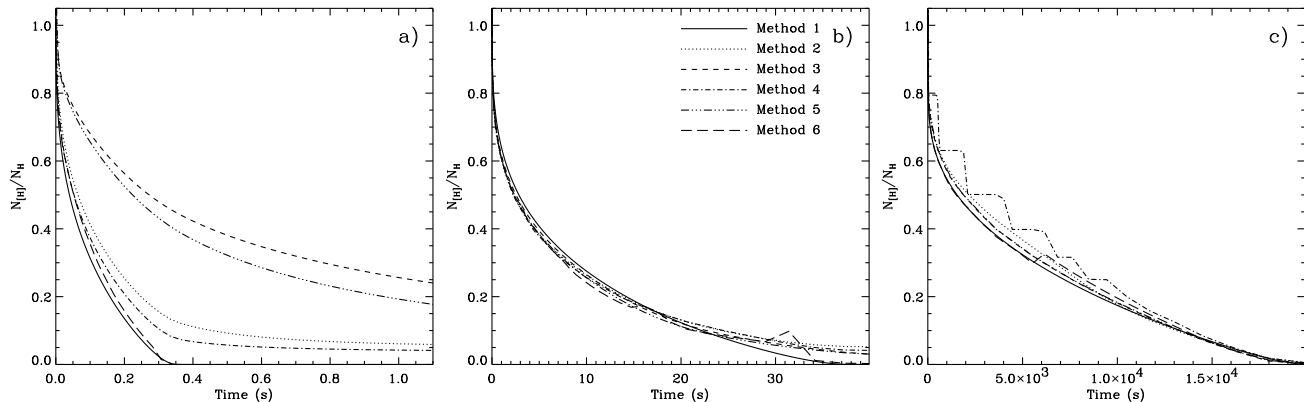


Figure 10. Comparison of the 6 methods for the evaluation of the effective N_H for various initial column densities. Results shown here are for a cloud with $R = 10^{18}$ cm, dust-to-gas ratio $d_k = 1$, and for a central source with $L = 10^{50}$ erg s^{-1} and $\alpha = 0$. Panel a), b) and c) show initial column densities $N_H = 10^{20}$, 10^{22} and 10^{24} cm^{-2} , respectively.

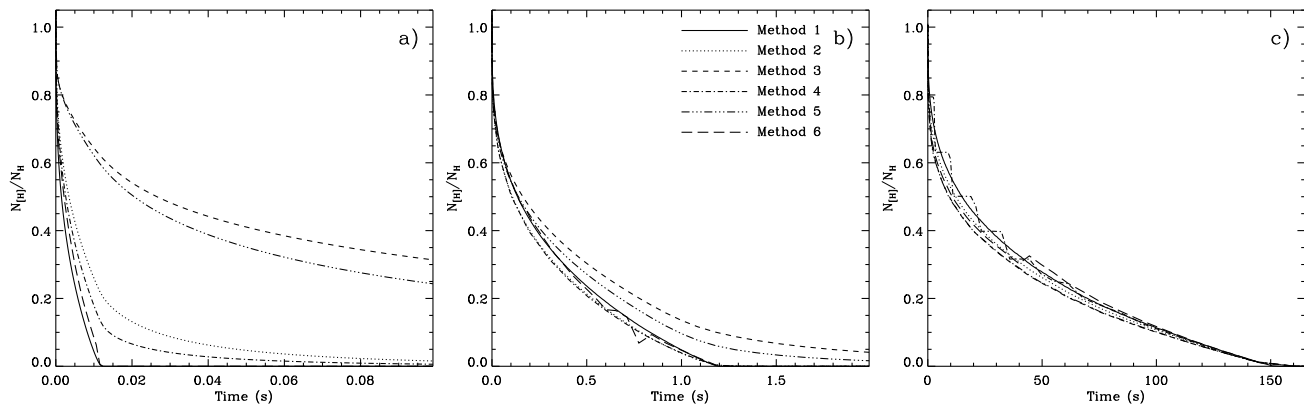


Figure 11. Same as Fig. 10 but for $\alpha = 0.5$.

about the evolution of the frequency dependent opacity with time, in a single indicator to be compared to observed spectra, especially if the signal to noise of them does not allow for the comparison with a detailed model. It is customary in the X-rays to quantify the soft X-ray absorption through the amount of column density of hydrogen $N_{[H]}$, under the assumption that the intervening medium is cold (see, e.g., Morrison & McCammon 1983).

The hydrogen column density is a good measure for the amount of absorption if the metallicity of the ISM is known and if the ISM is neutral. In fact, the measure of the column density is made through the comparison of the observed spectrum with an average photoabsorption cross section, computed under the assumption of solar metallicity for neutral elements. The assumption of a completely recombined gas is clearly not adequate in our case. We have developed several methods to derive an “effective column density” from the simulated spectra, which we will discuss and compare in detail below. The output of the various methods are also compared in Figs. 10 and 11 for several cloud geometries and two spectral indices of the ionizing continuum. Before doing that, it is however worth defining some quantities which are relevant when part of the atoms are completely stripped of their electrons and do not contribute to the absorption any more. We will call in the following N_X the column density of the element X irrespective of its ionization state, even if the element has lost all its electrons

and does not absorb photons any more. These quantities are a property of the cloud that is not modified by the central ionizing source. To indicate the quantity of absorbing ions of the element X , we use the notation $N_{X>}$, which is the column density of atoms and ions of the element X with at least one electron. Finally, we will use the symbol $N_{[H]}$ for the effective column density, i.e. the equivalent column of cold hydrogen that produces an amount of absorption comparable to what is obtained in the simulation. The following of this section is dedicated to find a good way to compute this quantity.

5.1 Real column density of absorbing hydrogen ($N_{H>}$)

As an output of our simulations, it is possible to derive the absorbing column density of HI as a function of time ($N_{H>}$). This is not really a prescription for comparing the observations with the simulations. Rather, the comparison of this $N_{[H]}$ with the other values derived with different methods is an indication of how the effective metallicity is changed by photoionization. Column densities derived with this method are shown with solid lines in Figs. 10 and 11 (Method 1).

5.2 Average opacity in selected bands

Following LP02, the effective column density can be computed by averaging the value of the opacity in a selected frequency range, and dividing the obtained value by the average of the cross section of a cold absorber in the same range:

$$N_{[H]} \equiv \left\langle \frac{\tau}{\sigma_0} \right\rangle_{[\nu_a, \nu_b]} \quad (5)$$

where τ is the frequency dependent opacity, σ_0 is the (frequency dependent) cross section of a cold medium with solar metallicity and $\langle \rangle_{[\nu_a, \nu_b]}$ represents the average over the frequency range ν_a, ν_b . The result is however highly dependent on the frequency range considered, so that different averages should be compared to measurements performed with different satellites. As an example we have computed the effective column densities in the range [0.2–1] keV (Method 2) and [2–10] keV (Method 3). The former is relevant for a typical X-ray instrument with good sensitivity in the sub-keV range (e.g. the BeppoSAX MECS and LECS), while the latter is more relevant for instruments such as the wide-field cameras on board BeppoSAX, whose sensitivity is relevant above 2 keV. The results of Method 2 and 3 are shown in Figs. 10 and 11 with a dotted and a dashed line, respectively.

5.3 Average transmitted flux in selected bands

It can be argued that an instrument is usually not sensitive to the value of the opacity, but to the transmitted flux. In other words, experimentally it is difficult, if not at all impossible, to distinguish between $\tau = 5$ and $\tau = 500$. For this reason, the equivalent absorbing column should be derived by averaging in selected bands the transmitted flux ratio, i.e. $e^{-\tau}$ rather than the opacity itself. The “effective column density” $N_{[H]}$ can therefore be implicitly defined as:

$$\langle e^{-\tau} \rangle_{[\nu_a, \nu_b]} = \langle e^{-\sigma_0 N_{[H]}} \rangle_{[\nu_a, \nu_b]} \quad (6)$$

where the meaning of symbols is the same as in Eq. 5. This method, even though more suited for a comparison with real data, will return a value of $N_{[H]}$ dependent on the frequency range over which the average is performed. Again, we performed the calculation in the [0.2–1] keV (Method 4) and [2–10] keV (Method 5) ranges. The results are shown in Figs. 10 and 11 with a dot-dash and a 3-dot-dash line, respectively.

5.4 Threshold opacity

An alternative way to estimate an “effective” column density that does not require the definition of a frequency range over which an average should be taken can be defined. The key of this method is to consider as more important the frequency range where the opacity is close to unity, i.e. where its presence is easily detectable and can be quantified. In fact, if the opacity is too small, there is no decrement in the transmitted flux while, if the opacity is too large, no flux is transmitted and only a lower limit can be set. Since the cross section for photoionization of a solar metallicity ISM is a steep function of frequency, the frequency at which the opacity has a fixed value is well constrained. We therefore computed the frequency at which the opacity is equal to 0.5

in our simulations and defined the effective column density $N_{[H]}$ as the inverse of the cross section of a cold absorber at the same frequency (Method 6). The results are plotted in Figs. 10 and 11 with a long-dashed line. The value 0.5 has been arbitrarily chosen. The inferred value of $N_{[H]}$ is however only slightly dependent on the choice of this number, which should be reasonably between 0.1 and 1. As can be seen from the figures, the disadvantage of this method is that in some points the value of $N_{[H]}$ has instabilities, related to the coincidences of the frequency at which the opacity is equal to 0.5 (or whatever selected value) with the photoionization threshold of an abundant element. In these cases, the cross column density of the cold absorber for the given opacity is not uniquely defined.

5.5 Discussion

The comparison of the different methods described above can be made from Figs. 10 and 11. For the case of an intermediate and large initial column density ($N_H \geq 10^{22} \text{ cm}^{-2}$), the 6 methods agree quite well, yielding comparable values of the effective column, irrespective of the spectral index and, therefore, also of the presence of dust. Method 4 is not particularly suited for large column densities, since in the low frequency range virtually no flux is transmitted for column densities larger than 10^{23} cm^{-2} . In the case of a relatively small initial column density, the methods based on averages at large frequencies (method 3 and 5) tend to give larger column densities, in particular in the case of a direct average of the opacity (Method 3). This is due to the fact that heavy metals are ionized with a slower speed with respect to hydrogen in the optically thin case. However, in these simulations, the opacity at large frequencies is very small and therefore methods 3 and 5 are not relevant since an instrument sensitive in the [2–10] keV regime would not detect any absorption.

6 FITTING SPECTRA

At any moment in time the observer will receive a transmitted spectrum that propagated through a medium under non equilibrium conditions. In fact, at any given radius, a condition of photoionization equilibrium cannot be reached, since the time during which the atoms and ions are subject to the ionizing continuum is much shorter than the recombination time scale (the burst duration is assumed to be 100 seconds). In addition, the ionization parameter $\xi \equiv L/(nr^2)$ is a function of the distance from the source. For these reasons, it is not strictly appropriate to model the observed GRB X-ray spectra with equilibrium models such as WABS⁵ or ABSORI⁶ within the XSPEC package (Arnaud 1996).

Despite these considerations, it is clearly an interesting issue whether the transmitted spectra derived in our simulations look like spectra from an highly ionized medium

⁵ The WABS photoionization opacity model (Morrison & McCammon 1983) assumes that the absorbing medium is neutral.

⁶ The ABSORI model (Done et al. 1992; Zdziarski et al. 1995) considers a warm absorbing medium, at a temperature T and illuminated by a steady power-law spectrum with uniform ionization parameter ξ .

or not. In other words: if the bursts explode inside giant molecular clouds, do we expect to see signatures of absorption from highly ionized atoms in their X-ray spectra? For example, the Chandra X-ray spectrum of GRB000210 (Piro et al. 2002) showed evidence of modest ionization (if at all) in its X-ray spectrum. Should this be considered an evidence against this burst taking place inside a dense environment?

To understand how much “ionized” may look the spectra predicted by our simulations, we have modelled a set of our synthetic spectra with the ABSORI model within the XSPEC package (Arnaud 1996). The fits were performed in the [0.3–20] keV range, assigning an error bar of 10% to the transmitted spectrum at all frequencies. An infinite resolution and flat effective area were assumed. The results are shown in Figs. 12 and 13 for a set of different geometries and dust content and two spectral indices. Again, here and in the following sections, we will consider simulations of an ionizing source with [1 eV–100 keV] luminosity $L = 10^{50}$ erg s $^{-1}$ turning on at the centre of a uniform spherical cloud and lasting for 100 s, after which is suddenly turned off. It can be seen that, even for big decrements in the observed absorbing column, the effective ionization parameter inferred by fitting the spectrum with a warm absorber model is very small. The presence of dust (dark lines in the figures) has the effect of making the transmitted spectra seem more ionized, in particular for the harder spectrum, in which some of the dust grains are preserved until the end of the simulation (see above). The noise in the figures is mainly due to the fact that since the error bars were arbitrarily assumed, there is no point in deriving error bars, and the fit was converging to different values for different time shots even if they had very similar χ^2 values. The real meaning of the figures is to show that none of the spectra are ever consistent even with the smallest ionization parameter for the clouds in the simulation, that was⁷ $\xi = 10^7$. The ionization parameter derived in the fit of a GRB spectrum with a warm absorber should therefore not be used to infer the physical conditions and geometry of the cloud that possibly surrounds the source.

7 APPARENT ELEMENT COLUMN DENSITIES AND RELATIVE ABUNDANCES

In this last section, before summarizing and discussing our results, we address the problem of the apparent metallicity of the absorber, should it be modelled with an absorber model in equilibrium conditions. Since the ionization time scales for different elements are different, the residual column density at time t will be strongly dependent upon the ionizing spectrum and the presence of dust. For example, Amati et al. (2000) used a cold absorber with variable metallicity to measure the iron abundance in the X-ray spectrum of GRB 990705 (see also Lazzati et al. 2001). They find in this way that iron must be 75 times more abundant than in the sun in order to reproduce the deep absorption through that was identified with an iron K_α photoionization edge.

Indeed their measurement is not an absolute measurement, but rather a comparison between the opacity in the

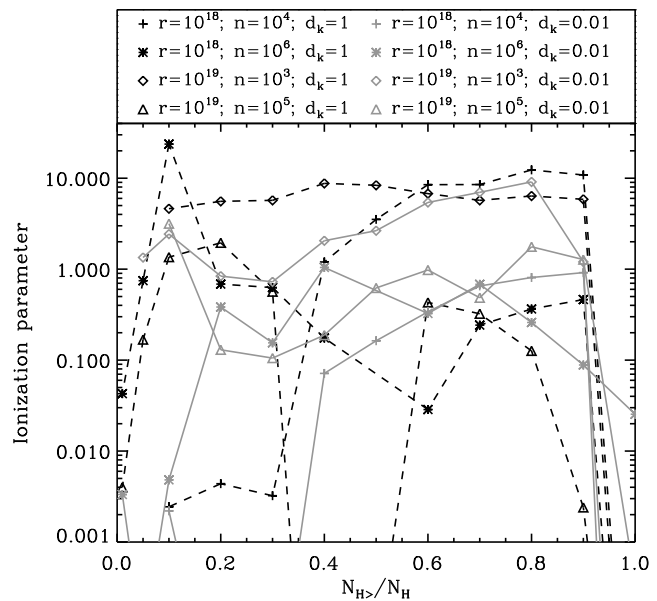


Figure 12. Apparent ionization parameter of the absorber as a function of the column density decrement for various absorbing clouds. The apparent ionization parameter is always small, even though the computed ionization parameter for the cloud outskirts is always very large, ranging from $\xi = 10^7$ to $\xi = 10^{10}$.

soft X-rays to the opacity at the frequency of the absorption edge. Since the edge was detected ~ 10 seconds after the GRB onset, the surrounding medium was heavily ionized. Therefore, the opacity in the soft X-ray band was not related to the column density of iron nuclei N_{Fe} , but rather to the fraction of nuclei with at least one electron $N_{\text{Fe} >}$. In addition, the depth of the trough was not compared to the hydrogen column density N_H but to the absorbing hydrogen column $N_{H >}$ (or to the oxygen $N_{O >}$, given the BeppoSAX WFC sensitivity range).

The ratio of the column density of ions of a particular element over the column density of nuclei of the same element in whatever ionization state (even completely stripped) is highly variable with time and can be derived from our simulations. Results for hydrogen, oxygen and iron are shown in Figs. 14 (for $\alpha = 0.0$) and 15 (same but for $\alpha = 0.5$). In each figure, the left panel shows the ratio of absorbing oxygen to absorbing hydrogen column densities (normalized to the initial “cold” value) versus the hydrogen column density at a given time over the initial one. The central panel shows the same ratios but for the iron-hydrogen ratio. Finally, the right panel, shows the iron-oxygen ratio.

The ratio of oxygen to hydrogen with at least one electron decreases as the global opacity of the medium decreases (i.e. as the time increases), showing that in most of the cases oxygen is ionized faster than hydrogen. Only for the “soft” spectra of Fig. 15 does the oxygen-to-hydrogen ratio increase with time. A more varied behavior is displayed by the iron ratio. For clouds with intermediate initial column densities ($N_H(0) = 10^{22}$ cm $^{-2}$; black lines) the fraction of iron to hydrogen increases with time, while for more opaque clouds ($N_H(0) = 10^{24}$ cm $^{-2}$; gray lines) the iron-to-hydrogen ratio tends to decrease at the beginning reversing then the trend at late times (when most of the original opacity has been

⁷ For AGN studies, it is more useful to adopt a different definition $U \equiv Q_H/(4\pi r^2 n c)$, in which case we have $U \sim 10^3$.

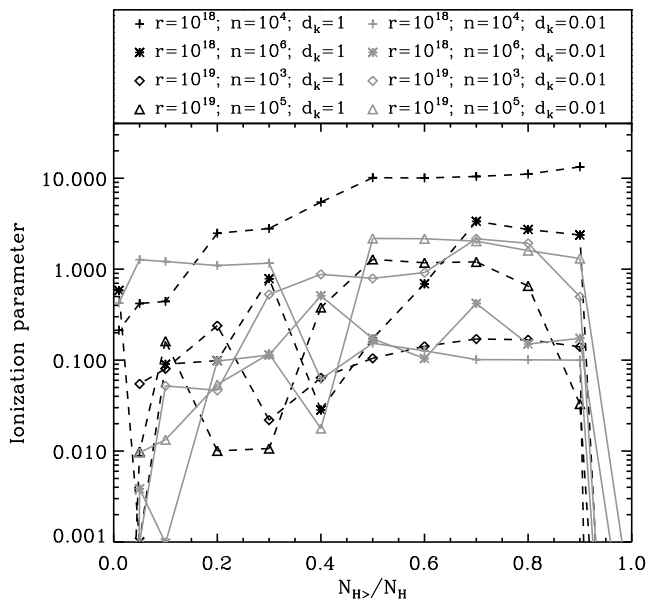


Figure 13. Same as Fig. 12 but for a spectral index $\alpha = 0.5$.

burned). This means that an observer will underestimate the oxygen abundance if fitting the X-ray spectrum with a cold absorber with variable abundances. On the other hand, the same observer may either overestimate or underestimate the iron richness depending on the initial column density of the cloud. In the case of GRB 990705, Amati et al (2000) compute the iron abundance for a cloud with initial column few $\times 10^{23}$ and find an iron abundance of ~ 75 when the column density is still comparable to the initial one. In this case we can see from Figs 14 and 15 that the iron richness was overestimated at most by a factor of a few. Even though the values of the ratios depend on the presence of dust, an interesting remark is that the most important parameter seems to be the initial column density, which determines the general trend of the evolution.

8 DISCUSSION AND CONCLUSIONS

We have analyzed with a dedicated code the time-dependent absorption properties of a cloud subject to a strong photon source that sets in at time $t = 0$ at its centre. The novelty of this paper consists in the fact that the presence of dust and its evaporation is fully taken into account by the code, allowing us to study if and how the presence of dust grains can affect the evolution of ionization and vice versa. This has great importance for variable sources such as GRBs and Seyfert galaxies, which are sometimes associated with unusual dust-to-gas ratios (Galama & Wijers 2001; Stratta et al. 2002), with variations of the column density (Risaliti et al. 2002; LP02) and with unusual extinction curves (Maiolino et al. 2001).

In this work we concentrated on the X-ray part of the spectrum, since the optical and infrared bands were addressed in a companion paper (Paper II). We study the evolution (evaporation) of the absorption in X-rays of a uniform cloud with solar metallicity for different dust contents, initial column density, cloud radius and hardness of

the ionizing spectrum. A source of [1 eV–100 keV] luminosity $L = 10^{50}$ erg s^{-1} is turned on at time $t = 0$ at the centre of the cloud.

We first concentrated on the effects that the presence of dust can have on the photoionization rate of metals. We find that, for hard spectrum sources, the presence of dust grains can have a big effect on the photoionization of metals (Fig. 5). In fact, if the soft photon flux is not large enough to destroy the dust grain by thermal sublimation, the surviving grains will effectively shield the entrained metals from photoionization (Fig 4), allowing them to survive in their neutral state for a long time (Fig 1). In the more extreme cases, it is possible that the ionizing flux completely ionizes all the atoms in the gaseous phase, leaving behind preferentially large graphite grains, that can contribute a sizable amount of absorption both at optical and X-ray wavelengths. The final conditions of the cloud depend on both the spectrum, luminosity and variability of the ionizing source as well as on the cloud size and column density (Fig 1, 6, 7).

We then study two issues related to observations and their modelling. It is in fact customary to model the absorption in the soft X-ray regime by means of equilibrium model for the absorbing medium. In the case we discuss, equilibrium is far from being reached, nevertheless it is useful, in order to exploit real observations, to understand if the predicted spectra look similar to those in equilibrium and how the column density of the absorbing material that would be measured does compare to the real one. We discuss the results of a fit with a cold absorber to our time dependent absorbed spectra (Fig 10, 11), and then show that a condition in which the absorber seems warm is never reached (Fig 12, 13).

We finally consider the observed column densities of the various elements, which are time dependent, since atoms completely stripped off their electrons do not contribute to the absorption and are therefore “invisible”. We find that these ratios are strong functions of time and that as a consequence the metallicities inferred from opacity ratios are not indicative of the pristine composition of the cloud (Fig 14, 15).

Present data do not allow for a detailed comparison with our numerical spectra. The only evidence of spectral evolution in the early phase of GRBs and afterglows comes from two detections of decreasing column density (Connors & Hueter 1998; Frontera et al. 2000), one variable absorption edge (Amati et al. 2000) and a puzzling evidence of variable (but not monotonic) column density (in’t Zand et al. 2001). All these detections belong to the 3σ realm and do not give much more information than their mere existence. In the near future, thanks to the launch of the Swift satellite in 2003, higher quality spectra will be available, allowing for a more secure detection of transient features and a more meaningful comparison with theoretical spectra.

ACKNOWLEDGMENTS

We are grateful to our referee, Luc Binette, for his careful report. We thank Luigi Piro for useful discussions and Tomaso Belloni for technical support. We acknowledge financial support from PPARC (DL) and from the Harvard Society of Fellows (RP).

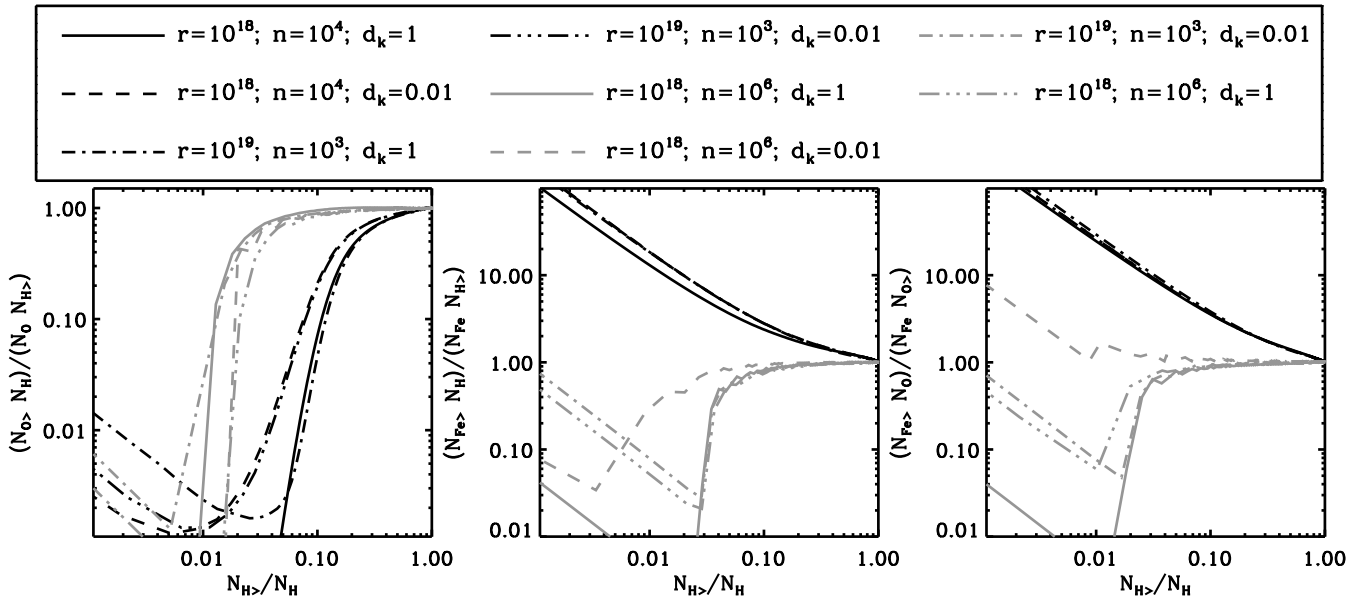


Figure 14. Evolution of the apparent abundance of oxygen and iron versus the evaporation of column. The figure shows, for a set of geometries and density of the absorbing cloud, the evolution of the absorbing column of oxygen and iron, the more easily detectable elements in X-rays. The cloud is centrally illuminated by a source of ionizing photons with $L = 10^{50}$ erg s^{-1} and $\alpha = 0.0$.

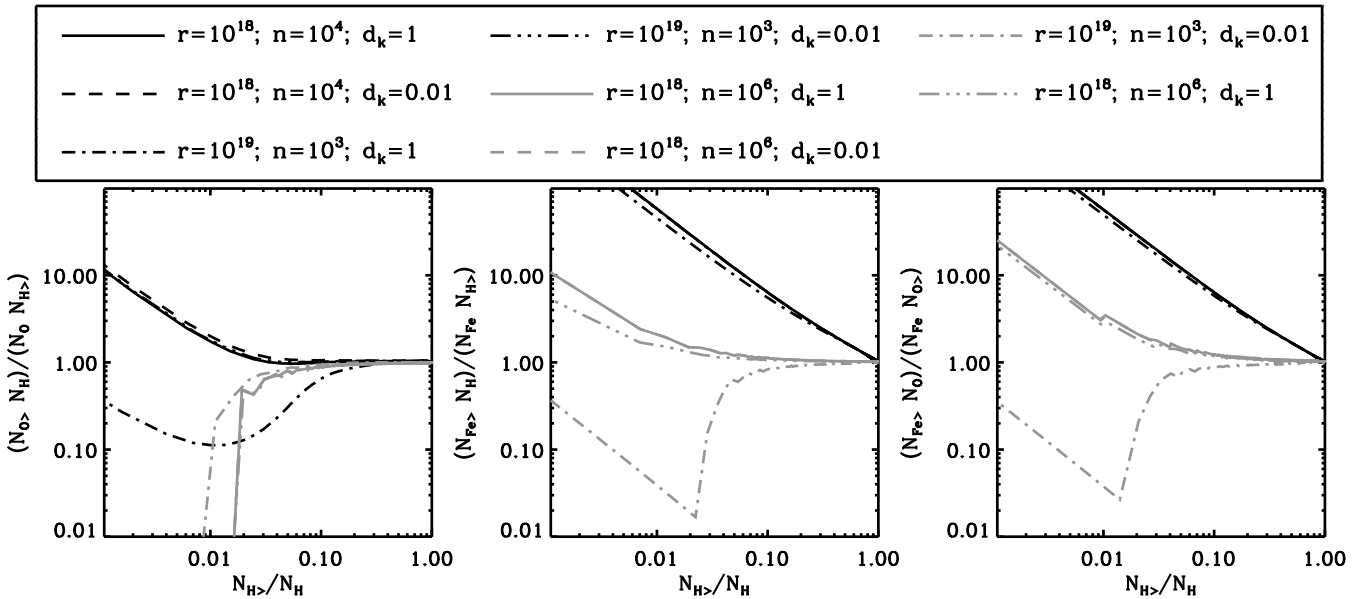


Figure 15. Same as Fig. 14 but for a spectral slope $\alpha = 0.5$.

REFERENCES

- Amati L., et al., 2000, *Science*, 290, 953
 Anders, E., & Grevesse, N. 1989, *Geochim. Cosmochim. Acta*, 53, 197
 Arnaud, K. A., 1996, in Jacoby G. H., Barnes J., eds, ASP Conf. Ser. Vol. 101, *Astronomical Data Analysis Software and Systems V*. Astron. Soc. Pac., S. Francisco, p. 17
 Connors A., Hueter G. J., 1998, *ApJ*, 501, 307
 Done, C., Mulchaey, J. S., Mushotzky, R. F., & Arnaud, K. A. 1992, *ApJ*, 395, 275
 Draine, B. T. & Hao, L. 2002, *ApJ*, 569, 780
 Fruchter A., Krolik J. H. & Rhoads J. E. 2001, *ApJ*, 563, 597
 Frontera F., Amati L., Costa E., et al., 2000, *ApJS*, 127, 59
 Galama, T. & Wijers, R. A. M. J. 2001, *ApJ*, 549, 209
 in't Zand J. J. M., Kuiper L., Amati L., et al., 2001, *ApJ*, 559, 710
 Laor, A. & Draine, B. T. 1993, 402, 441
 Lazzati, D., Perna, R., 2002, *MNRAS*, 330, 383 (LP02)
 Lazzati, D., Perna, R., & Ghisellini, G. 2001, *MNRAS*, 325, L19
 Lazzati, D., Ghisellini, G., Amati, L., Frontera, F., Vietri, M., & Stella, L. 2001, *ApJ*, 556, 471
 Maiolino R., Marconi A., Salvati M., Risaliti G., Severgnini P., Oliva E., La Franca F., Vanzani L., 2001, *A&A*, 365, 28
 Mathis J. S., 1990, *ARA&A*, 28, 37
 Morrison R., McCammon D., 1983, *ApJ*, 270, 119

- Perna, R., Loeb, A. 1998, ApJ, 501, 467
Perna, R., Raymond, J., & Loeb, A. 2000, ApJ, 533, 658
Perna R., Lazzati D., 2002, ApJ, 580, 261 (Paper I)
Perna R., Lazzati D., Fiore F., ApJ in press (astro-ph/0211235;
Paper II)
Piro, L., Frail, D. A., Gorosabel, J., et al., 2002, ApJ, 57, 680
Raymond J. C., 1979, ApJS, 39, 1
Reilman, R. F. & Manson, S. T. 1979, ApJS, 40, 815
Risaliti G., Elvis M., Nicastro F., 2002, ApJ, 571, 234
Savage B. D., Mathis J. S., 1979, ARA&A, 17, 73
Schwarz J., 1973, ApJ, 182, 449
Stratta, G. et al. 2002, ApJ submitted
Verner, D. A., Yakovlev, D. G. 1995, A&AS, 109, 125
Waxman, E.; Draine, B. T. 2000, ApJ, 537, 796
Zdziarski, A. A., Johnson, W. N., Done, C., Smith, D., &
McNaron-Brown, K. 1995, ApJ, 438, L63